



Effects of unfolded and intercalated halloysites on mechanical properties of halloysite–epoxy nanocomposites

Youhong Tang^{a,b}, Shiqiang Deng^a, Lin Ye^{a,*}, Cheng Yang^c, Qiang Yuan^d, Jianing Zhang^a, Chengbi Zhao^b

^a Centre for Advanced Materials Technology, School of Aerospace, Mechanical and Mechatronic Engineering, The University of Sydney, NSW 2006, Australia

^b Centre for Advanced Marine Materials, School of Civil Engineering and Transportation, South China University of Technology, Guangzhou 510640, China

^c Department of Mechanical Engineering, The Hong Kong University of Science and Technology, Clear Water Bay, Kowloon, Hong Kong, China

^d CSIRO Manufacturing & Infrastructure Technology, 37 Graham Rd., Highett, Vic 3190, Australia

ARTICLE INFO

Article history:

Received 6 September 2010

Received in revised form 29 November 2010

Accepted 2 December 2010

Available online 5 December 2010

Keywords:

A. Particle-reinforcement

B. Fracture toughness

C. Microstructure

D. Mechanical testing

ABSTRACT

Phenylphosphonic acid (PPA) was used to unfold a unique tubular clay mineral, halloysite. By varying the durations of PPA treatment, halloysites with different levels of enfolding and intercalation were obtained. Halloysites, particularly with the unfolded and intercalated halloysites, were effective additives in increasing the fracture toughness of the cured epoxies without sacrificing their basic properties. Fracture toughness of composites was increased with increasing intercalation levels of halloysite, with the improvement being 78.3% in K_{IC} for the composite containing 10 wt.% of the fully PPA-intercalated and unfolded halloysite. There was a substantial increase in the contact area between halloysite and epoxy, and as a result the morphology changed from nanotubes to nano-platelets in the composites with the treated halloysites. The treated halloysites achieved a better dispersion in epoxy and promoted the formation of a large number of micro-cracks and plastic deformations in the interfaces, resulting in an improvement in fracture toughness.

© 2010 Elsevier Ltd. All rights reserved.

1. Introduction

Nano-sized inorganic particles as modifiers for brittle polymers such as polystyrene, poly(methyl methacrylate) and epoxies have been intensively studied in the past decades, with the aim of achieving a synergistic improvement in both toughness and rigidity [1–5]. Organically modified montmorillonite (MMT) has given rise to extensive research efforts as a candidate additive for toughness enhancement of polymers. In those efforts, MMT particles were intercalated or exfoliated and combined with polymers such as epoxies to form nanocomposites. When a MMT nanocomposite was subjected to a load, micro-cracks initiated between two weakly bonded clay layers and the growth of the micro-cracks was resisted by the MMT platelets, which led to high fracture energy [1,2]. Carbon nanotube (CNT) has also been considered as an ideal modifier due to its excellent mechanical strength and large aspect ratio [3,4]. The amino-functionalized multiwalled CNT was previously reported to double the impact strength of an epoxy [3].

In recent years, halloysite particles have been investigated as an alternative type of additive for polymers [6–15]. Halloysite is a naturally occurring aluminosilicate, $\text{Al}_2\text{Si}_2\text{O}_5(\text{OH})_4 \cdot 2\text{H}_2\text{O}$, chemically similar to kaolinite, dickite or nacrite, differing mainly in the mor-

phology of crystal. Halloysite is a layered clay mineral, consisting of one alumina octahedron sheet and one silica tetrahedron sheet in a 1:1 stoichiometric ratio. The halloysite particle can adopt a variety of morphologies, but the most common form is an elongated hollow tubular structure with a large aspect ratio, similar to that of CNTs, due to its structural defects, particularly in the layer stacking of the neighboring alumina and silica layers, and their hydrated waters [16]. Halloysite particles are readily obtainable and are much cheaper than other nanoparticles such as CNTs. More importantly, the unique crystal structure of halloysite nanotubes resembles that of CNTs, and therefore halloysite particles may have the potential to provide cheap alternatives to expensive CNTs because of their tubular structure in nano-scale. Moreover, due to its similarity to other layered clay minerals such as MMT, halloysite has the potential to be further intercalated or exfoliated chemically or physically [6]. In previous studies [7–9] the incorporation of a small amount of halloysite particles (5–15 wt.%) into epoxy resins was found to noticeably increase the mechanical performance of the materials, including their strength, modulus and fracture toughness, without sacrificing other properties such as glass transition temperature (T_g). With the use of conventional mechanical mixing methods, most of the halloysite existed in the epoxies in the form of particle clusters rather than individual particles, but the epoxy resin could penetrate fully into the clusters [8]. Increased fracture toughness was mainly attributable to mechanisms such as crack bridging, crack deflection and plastic

* Corresponding author. Tel.: +61 2 93514798; fax: +61 2 93513760.

E-mail address: lin.ye@sydney.edu.au (L. Ye).

deformation of the epoxy around the halloysite particle clusters. Halloysite particle clusters could interact with cracks at the crack front, resisting the advance of the crack and resulting in an increase in fracture toughness [8,9]. The ability of halloysite to be intercalated or exfoliated by salts and organic compounds has been reported [16–18]. Intercalation and/or exfoliation of halloysite with inorganic and organic compounds may have significant potential applications, similar to those of intercalated MMT. There has been little investigation, however, of the use of intercalated halloysite as a filler for polymers. In our previous study [9], X-ray diffraction analysis of treated halloysite particles using three chemicals, namely potassium acetate (CH_3COOK) (PA), Z-6020 silane [N-(β -aminoethyl)- γ -aminopropyltrimethoxysilane] and cetyl trimethyl ammonium chloride [$\text{CH}_3(\text{CH}_2)_{15}\text{N}(\text{Cl})(\text{CH}_3)_3$] (CTAC), showed that the treatments did not result in shifting the peak at 12.3° (corresponding basal spacing of 7.2 \AA) to the left, indicating that these chemicals were unable to intercalate halloysite under the experimental condition utilized in the study, though the resulting halloysite–epoxy composites exhibited improved properties compared to the neat resin [9].

In the current study, an attempt was made with a different chemical, phenylphosphonic acid (PPA), to obtain partially or fully unfolded and intercalated halloysite particles, which depended on treatment duration. The treated halloysite particles were then combined with an epoxy to form intercalated nanocomposites. Characterization of the resultant halloysite–epoxy composites was then conducted to elaborate the effects of the unfolded and intercalated halloysite on the mechanical properties, especially the fracture behaviors, of the composites.

2. Experimental

2.1. Chemical treatment of halloysite

The halloysite particles used in this study were purchased from Sigma–Aldrich Australia. In the chemical treatment of the halloysite particles, 280 g of PPA (analytical grade, Sigma–Aldrich Australia) was first dissolved in water (3 l) and 152.4 g of halloysite was then added into the solution. The mixture was refluxed in a sealed glass beaker on a hot plate at 100°C under vigorous magnetic mixing using a ceramic stirring bar for certain periods of time, namely 25, 50 and 100 h. After cooling to room temperature, the mixture was filtered, washed with distilled water at least five times and dried at room temperature in a ventilation hood for more than 7 days until no further weight loss was detected. The process of the PPA treatment is shown in Scheme 1.

2.2. Preparation of halloysite–epoxy nanocomposites

The as-received and the treated halloysite particles with different treatment times were separately combined with a diglycidyl ether of bisphenol A (DGEBA) epoxy resin, Araldite-F (Ciba-Geigy, Australia) to form composites. Both the as-received and the PPA-treated halloysite particles in 10 wt.% were separately added into the epoxy resin, by means of a mechanical mixer, stirring at 100°C for 5 h to obtain homogeneous mixtures. The mixtures were then degassed in a vacuum oven (about -100 kPa) for at least

30 min. After that, a hardener, Piperidine (Sigma–Aldrich, Australia), was added to the mixtures in a ratio of 100:5 by weight, while stirring slowly. Following further degassing for 10 min the vacuum was released and the liquid mixtures were cast into the specimen cavities of preheated silicon rubber moulds and cured at 120°C for 16 h. For the designated mechanical tests, different rubber moulds were prepared to produce tensile and compact tension specimens. When the specimens had been cooled and removed from the moulds they were milled using a surface grinder on both top and bottom surfaces to ensure flatness of specimens and, most importantly, to remove possible oversized halloysite particle aggregates, which could sink to the bottom surfaces during curing, as reported previously [8]. As a baseline for comparison, specimens were also prepared for the neat epoxy.

2.3. Characterization

Wide angle X-ray diffraction (WAXD) was conducted on the halloysite and halloysite–epoxy nanocomposites using an X-ray diffraction unit (Model D5000, Siemens, Germany) with $\text{Cu K}\alpha$ radiation (wavelength = 1.54056 \AA).

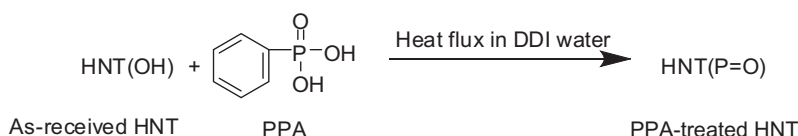
A Fourier transform infrared spectrometer (FTIR, Bio-Rad FTS 6000, USA) was used at room temperature with transmission mode to identify the possible chemical reactions between halloysite and PPA. Spectral resolution of the FTIR was maintained at 2 cm^{-1} . Dry nitrogen gas was used to purge the sample compartment to reduce the interference of water and carbon dioxide in the spectrum. The halloysite was mixed with potassium bromide (KBr) and pressed to form a thin film of about $300 \mu\text{m}$ in thickness prior to examination.

Nitrogen adsorption/desorption isotherms at 77 K were measured with a Quantachrome Autosorb 1 MP instrument (USA). The standard Brunauer–Emmett–Teller (BET) model was used to calculate the specific surface area (SSA) of the as-received and PPA-treated halloysites.

Transmission electron microscopy (TEM) images, electron diffraction (ED) patterns and energy dispersive X-ray (EDX) element analysis (EA) spectra of the halloysite and halloysite–epoxy nanocomposites were obtained using a transmission electron microscope (JEOL 2010, Japan) at 200 kV. For the preparation of the TEM specimens, halloysite particles were dispersed in ethanol, and one droplet of the solution was dropped onto carbon coated Cu grids for TEM observation after evaporation of the solvent. Halloysite–epoxy nanocomposites were ultramicrotomed using glass knives on an ultra-cut microtome (Leica ultracut-R ultramicrotomed, Germany) to produce thin sections with a nominal thickness of 100 nm. The sections were transferred onto Cu grids for TEM observation.

Scanning electron microscopes (Philips XL30 SEM, the Netherlands and Zeiss ULTRA Plus Field Emission SEM, Germany) were utilized to identify the morphology of halloysite particles, the homogeneity of halloysite particles in the epoxy nanocomposites, and failure modes of compact tension (CT) fracture specimens.

Thermal stability analysis was carried out using a Hi-Res TGA 2950 thermogravimetric analysis apparatus (TA instruments, USA). The tests were carried out in air with a heating rate of $20.0^\circ\text{C}/\text{min}$ from 50.0°C to 600.0°C , followed by isotherm for 15 min at 600.0°C before cooling.



Scheme 1. Modification of halloysite particles by phenylphosphonic acid (PPA).

The glass transition temperature (T_g) of the cured neat epoxy and the halloysite–epoxy nanocomposites was determined by a dynamic mechanical analyzer (DMA 2980, TA Instruments, USA) with temperature scanning from ambient temperature to 150 °C at a heating rate of 3 °C/min. A three-point bending fixture was used for the DMA measurements. A displacement amplitude of 10 μm was alternately applied with a frequency of 1 Hz for all DMA measurements. At least three specimens were tested for each group, and the average value of T_g determined from the peak of the $\tan\delta$ vs. temperature curves was obtained.

A universal material testing machine (Instron, Mode 5567, USA) was used for all mechanical characterizations including tension and fracture toughness tests. All mechanical tests were conducted at room temperature.

The fracture toughness of the cured neat epoxy and halloysite–epoxy nanocomposites was measured using the compact tension (CT) specimens according to ASTM D5045. A CT specimen has a nominal dimension of 48 mm \times 48 mm \times 10 mm. To minimize the effects of residual stress and residual plastic deformation around the pre-crack tip, a sharp pre-crack was introduced to each CT specimen by inserting a fresh razor blade at the tip of the machined crack and tapping gently with a light hammer [19]. A loading rate of 2 mm/min was adopted for all fracture tests, as recommended by ASTM D5045-99. As there are strict requirements for specimen geometry and crack length for the accurate measurement of the fracture toughness using CT tests according to the ASTM criteria, only those specimens which fulfilled the condition $a/W = 0.45\text{--}0.55$ (a is the pre-crack length and W is the distance between the centre of the loading pin to the edge of the CT specimen) were used to calculate the critical stress intensity factor (K_{1C}). At least 8 CT specimens were successfully tested for each group of materials.

Tensile tests were conducted to measure the basic material properties of the cured neat epoxy and the halloysite–epoxy composites. Tensile specimens had a dog-bone shape as required by ASTM D638-99, with a constant cross-section of 13 \times 5 mm at the gauge length region. An extensometer with a gauge length of 50 mm was attached to the surface of the tensile specimen to determine the axial strain. A loading rate of 1 mm/min was selected for all tensile tests. At least five specimens were successfully tested for each group.

3. Results and discussion

3.1. Intercalation of halloysite with PPA

X-ray diffraction spectra of halloysite particles with different PPA treatment durations are shown in Fig. 1. The basal spacing [001] of the as-received halloysite was approximately 7.2 Å, based on the diffraction angle for the peak at $2\theta = 12.3^\circ$. After PPA treatment for 25 h a new diffraction peak appeared at $2\theta = 5.8^\circ$, which was due to the PPA intercalation to halloysite interlayer positions, causing expansion of the layers in the direction perpendicular to the base plane, with a final basal spacing of 15.1 Å, which is the largest basal spacing ever reported [16]. With increase in the duration of PPA treatment the peak intensity at $2\theta = 5.8^\circ$ was gradually enhanced, indicating an increase of the intercalated particles. With a treatment time of 100 h, the peak at $2\theta = 12.3^\circ$ almost disappeared, indicating that all the halloysite particles were almost fully intercalated. The intercalation levels of halloysite by PPA were estimated by comparing the relative intensities at $2\theta = 5.8^\circ$ and 12.3° , as shown in Table 1.

Fig. 2 shows the FTIR spectra of the as-received halloysite and that with PPA treatment for 50 and 100 h, respectively. The characteristic peak appearing at 1155 cm^{-1} for the PPA-treated halloy-

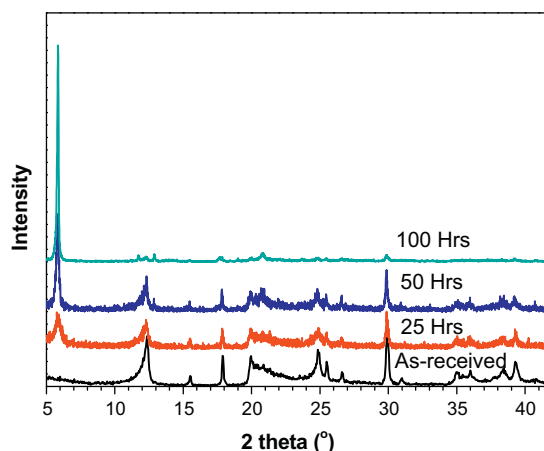


Fig. 1. X-ray diffraction patterns of halloysite particles treated by phenylphosphonic acid (PPA) for different durations. (For interpretation of the references to colour in this figure legend, the reader is referred to the web version of this article.)

Table 1

Intercalated levels of halloysite particles obtained by comparing X-ray diffraction intensities at $2\theta = 5.8^\circ$ and 12.3° .

Duration of PPA treatment (h)	Nominal intercalated level (%)	Weight loss after heating up to 600 °C (%)	PPA content (%)
0	0	13.9	0
25	54	–	–
50	61	19.0	5.1
100	100	27.6	13.7

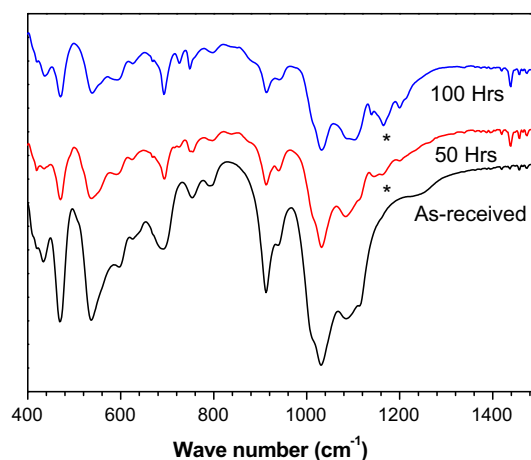


Fig. 2. FTIR spectra of halloysite particles before (as-received) and after PPA treatment for 50 and 100 h (*P=O stretching vibration peak). (For interpretation of the references to colour in this figure legend, the reader is referred to the web version of this article.)

sites is obviously a P=O stretching peak, providing evidence of PPA residence on the halloysite surfaces in the treated specimens.

As shown in Fig. 3a, the as-received halloysite particles used in this study were basically in the form of short small tubes (nanotubes) with a length of 100–2000 nm and a diameter of 50–150 nm, geometrically similar to multiwalled CNTs. However, long CNTs always tend to entangle with each other, forming agglomerates that make it difficult to disperse them homogeneously in polymers. In contrast, short halloysite nanotubes (HNTs) are straight and individually separate without entanglement, which potentially

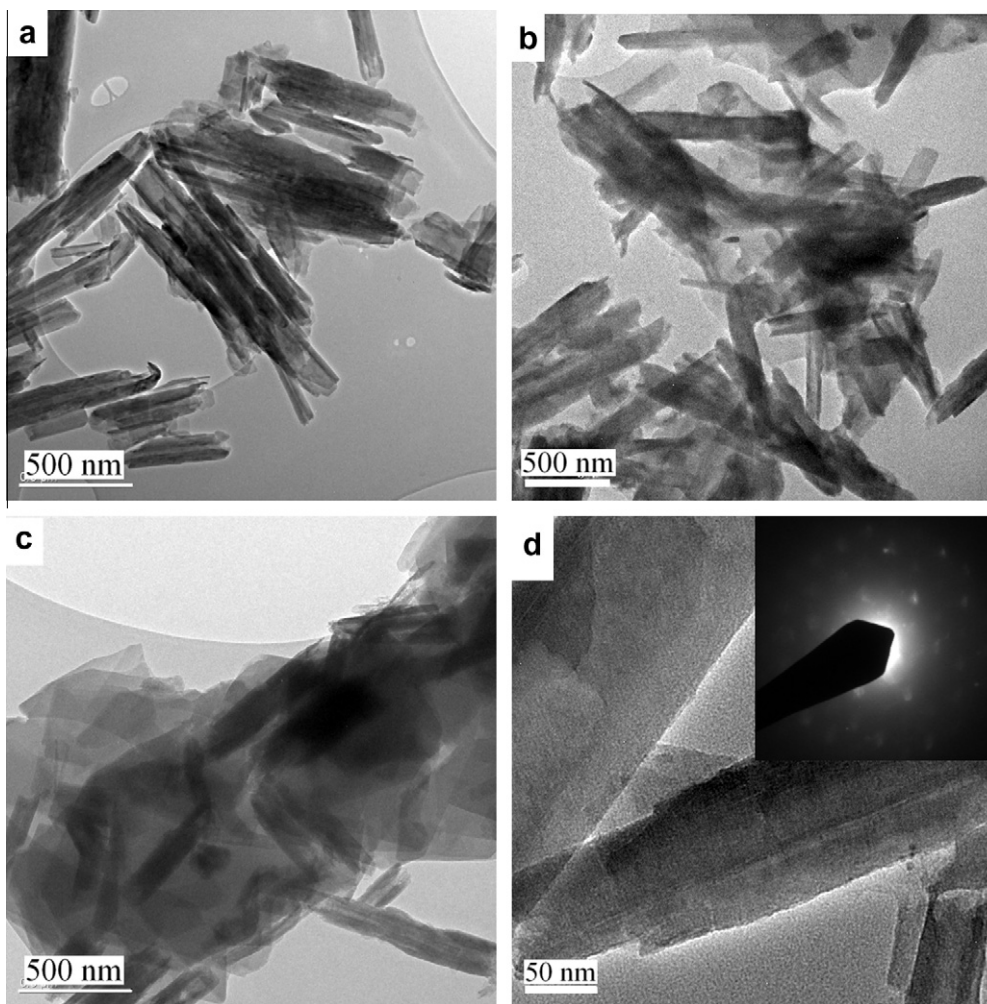


Fig. 3. TEM images of halloysite particles treated by PPA for different durations. (a) as-received; (b) and (c) after PPA treatment for 50 and 100 h; (d) electron diffraction pattern after PPA treatment of 50 h, showing the crystal structure of halloysites.

make it easy to obtain good dispersion of HNTs in viscous polymers. Indeed, HNTs are in the form of rolled tubes [20] consisting of a number of aluminosilicate sheets, curved and closely packed. After the PPA intercalation, the large layer expansion would unfold some or most of the curved tubes, which could provide the opportunity for intercalation of layers or exfoliation of individual layers, similar to that for organically modified MMT. As shown in Fig. 3b, after PPA treatment of 50 h, some flat halloysite platelets can be observed, and with PPA treatment of 100 h most of the halloysite particles became platelets, with some even being dispersed flakes (exfoliated aluminosilicate sheets). The results obtained from the X-ray diffraction analysis, shown by the electron diffraction pattern in insets of Fig. 3d, confirmed that the intercalated halloysite still maintained its crystalline structure after the PPA treatment. Element analysis spectra in Fig. 4a–c were obtained by the energy dispersive X-ray (EDX) spectrometer attached to the TEM, and they proved that the element phosphorus existed in the treated samples, indicating that PPA was either intercalated in interlayers or on the surfaces of halloysite particles.

The results of thermogravimetric analysis are shown in Fig. 5 for the as-received and PPA-treated halloysite samples. It can be seen that the as-received halloysite is relatively stable up to 400 °C, and a weight loss of 13.9% occurs after temperature reaches 600 °C, representing the removal of the interlayer water. Compared with the as-received halloysite sample, there is some extra weight loss for the PPA-treated halloysite samples during the heating process

up to 600 °C, probably caused by decomposition of PPA in the halloysite samples. The total weight loss is approximately 27.6% after temperature reaches 600 °C for the sample treated for 100 h, so that there is approximately 13.7% of PPA, either intercalated to interlayers or attached on halloysite surfaces in the fully intercalated halloysite sample. The PPA contents in the treated halloysites with two different durations of treatment are also shown in Table 1.

3.2. Halloysite–epoxy composites

WAXD patterns of halloysite–epoxy composite samples are shown in Fig. 6. Clearly, a peak at $2\theta = 11.9^\circ$ can be seen for the as-received untreated halloysite–epoxy composite while the peak at $2\theta = 5.8^\circ$ is absent. Broad low peaks appear at both $2\theta = 5.8^\circ$ and $2\theta = 11.9^\circ$ for the halloysite–epoxy composite sample with the halloysite treated for 25 h using PPA. With increasing treatment time, the peaks at $2\theta = 5.8^\circ$ become clearer and sharper, whereas the peak at $2\theta = 11.9^\circ$ almost disappears for the composites with halloysite treated for 50 and 100 h, indicating that the intercalated structure of the halloysite is still preserved in the halloysite–epoxy composites.

The tensile properties of the cured neat epoxy and the halloysite–epoxy composites are summarized in Table 2. Typical strain vs. stress curves of the tensile specimens of neat epoxy and halloysite–epoxy composites with PPA treatments are shown in Fig. 7. It

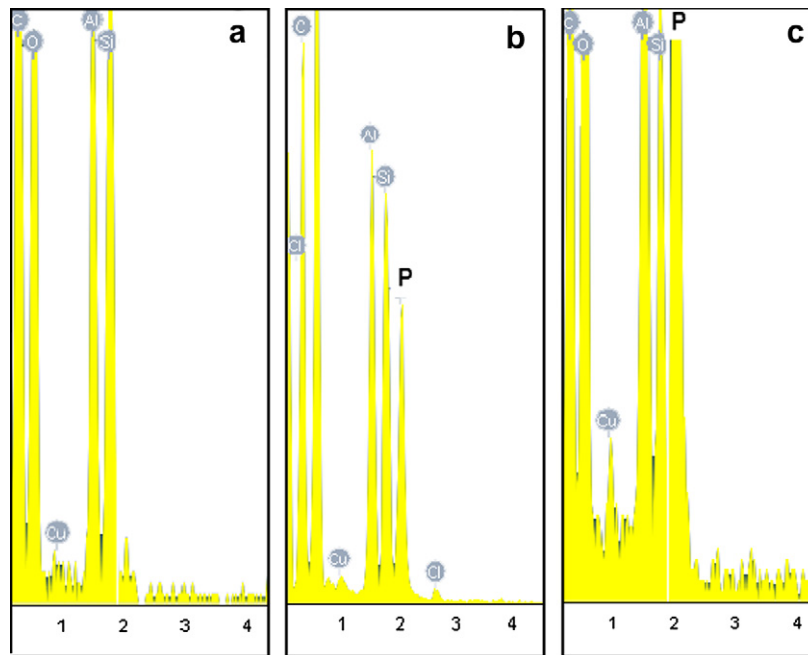


Fig. 4. EDX spectra of halloysite treated using PPA. (a) as-received; (b) after 50 h of PPA treatment; and (c) after 100 h of PPA treatment; peaks for element phosphorus in (b) and (c) are indicated by P. (For interpretation of the references to colour in this figure legend, the reader is referred to the web version of this article.)

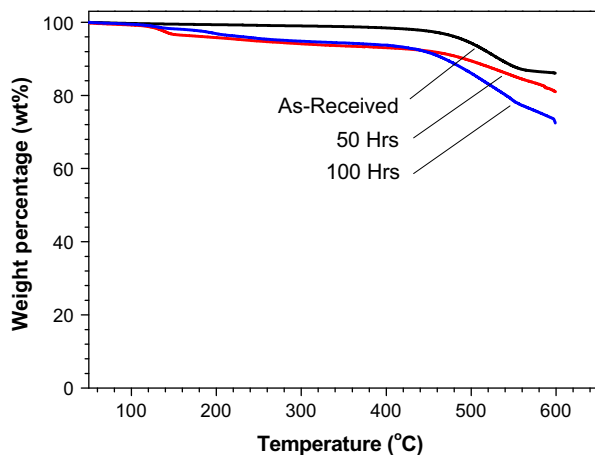


Fig. 5. TGA data in air for halloysite particles with and without PPA treatment. (For interpretation of the references to colour in this figure legend, the reader is referred to the web version of this article.)

is evident that the composites containing halloysite nanoparticles have acquired an increase in both strength and modulus compared to those of the cured neat epoxy. These property enhancements were attributed to the reinforcing effect of halloysite particles in the epoxy matrix. However, with the use of PPA-treated halloysite particles, there was less enhancement in the tensile strength and modulus, probably due to the fact that the morphology of most of the halloysite particles changed from a tubular shape into platelets, accompanied by some reduction of their aspect ratios after the PPA treatment.

The glass transition temperatures of the neat epoxy and halloysite-epoxy composite samples were defined from the $\tan\delta$ peaks in DMA results and the average values are also shown in Table 2. The increased T_g of the halloysite-epoxy composites containing PPA-treated halloysite particles is probably attributable to the fact that the flat shapes of the intercalated halloysite particles increased the

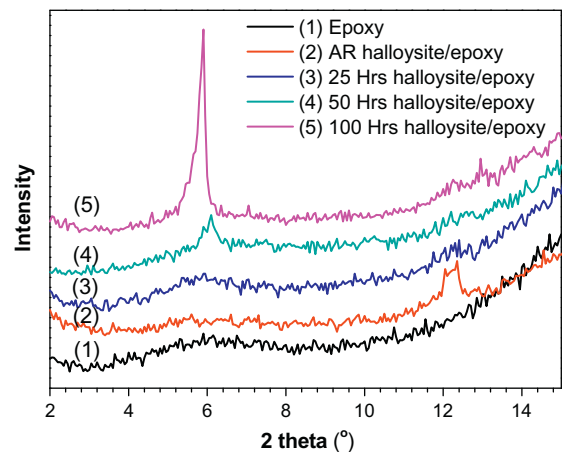


Fig. 6. X-ray diffraction patterns of halloysite-epoxy composites with halloysite particles treated with PPA for different durations. (For interpretation of the references to colour in this figure legend, the reader is referred to the web version of this article.)

effective surface area of the halloysite in contact with the epoxy matrix, compared to the as-received halloysite. This speculation is confirmed by the standard BET test [21], where the as-received halloysite had a SSA of 21.22 m²/g whereas the 100-h PPA-treated halloysite had a SSA of 41.13 m²/g. The 100-h PPA-treated halloysite had almost double the surface area of the as-received halloysite, corresponding to a simple scenario when a tube (in which the inner surface is inaccessible) is unfolded to create double the surface area. The increased surface area created further constraint to the mobility of the epoxy polymer chains, confirmed by a slightly increased T_g .

However, the most important advantage for the use of intercalated halloysite in epoxy-based nanocomposites is the clear increase in their fracture toughness. Fig. 8 shows a set of typical load-crack opening displacement (COD) curves obtained from CT tests for the cured neat epoxy and halloysite-epoxy

Table 2
Tensile properties and glass transition temperatures of neat epoxy and halloysite(10.0 wt.%)–epoxy composites.

Samples	Strength (MPa)	Modulus (GPa)	Strain at peak load (%)	T_g (°C)
Neat epoxy [8]	62.6 ± 0.6	2.90 ± 0.12	4.49 ± 0.12	95.5 ± 1.9
As-received	64.3 ± 0.2	3.40 ± 0.26	4.09 ± 0.11	97.1 ± 1.0
PPA-treated (25 h)	63.4 ± 1.1	3.16 ± 0.26	4.88 ± 0.45	100.7 ± 1.8
PPA-treated (50 h)	63.8 ± 0.3	3.14 ± 0.07	4.70 ± 0.12	102.6 ± 3.0
PPA-treated (100 h)	62.6 ± 0.9	3.33 ± 0.16	4.52 ± 1.18	108.2 ± 3.2

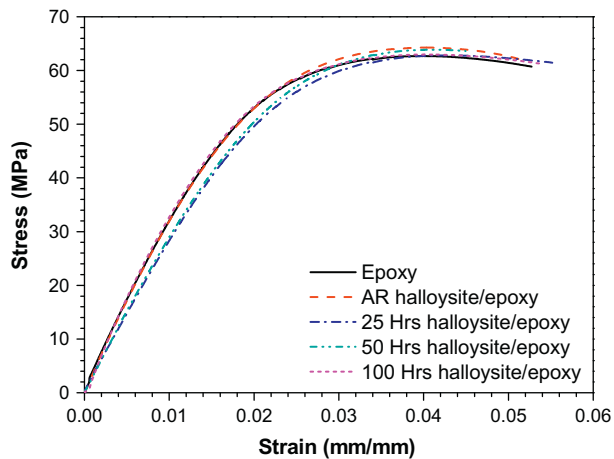


Fig. 7. Typical tensile stress vs. strain curves of neat epoxy and halloysite–epoxy composites.

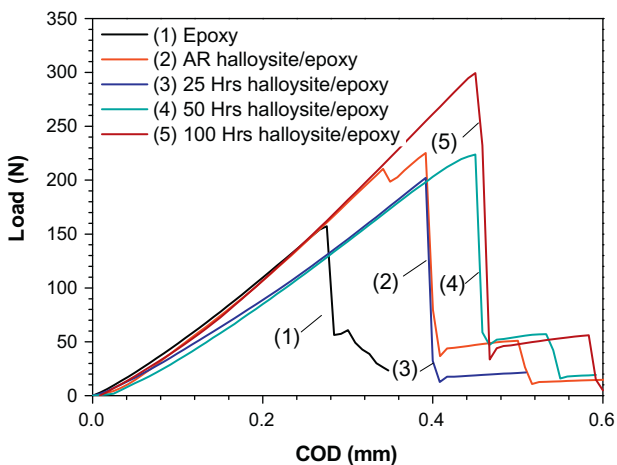


Fig. 8. Typical load vs. COD curves of the neat epoxy and halloysite–epoxy composites (CT specimens with initial crack length of about 20 mm).

nanocomposites, when the crack length of the specimens was the same. It can be seen that although both the pure epoxy and the PPA-treated halloysite–epoxy composites showed unstable crack propagation when the maximum load was reached, the maximum loads for the epoxies with halloysite were clearly higher than that for the neat epoxy. As shown in Table 3, the magnitudes of the critical stress intensity factor (K_{IC}) of the epoxy composites were significantly improved after halloysite of 10 wt.% was incorporated, particularly with the use of PPA-treated halloysite. For the epoxy with as-received halloysite, the improvement in K_{IC} was 25.0%, from 0.92 MPa m^{1/2} (neat epoxy) to 1.15 MPa m^{1/2}. For the epoxy with 25-h PPA-treated halloysite, the increase was approximately 23.9% (with the magnitude of 1.14 MPa m^{1/2}), and with the use of the halloysite treated for prolonged durations (50 and 100 h), K_{IC}

Table 3
Fracture toughness (K_{IC}) of the neat epoxy and the halloysite (10.0 wt.%)–epoxy composites.

Sample	K_{IC} (MPa m ^{1/2})	Improvement (%) (compared with neat epoxy)
Neat epoxy [9]	0.92 ± 0.04	0.0
Halloysite (10 wt.%)–epoxy		
As-received	1.15 ± 0.08	25.0
PPA-treated (25 h)	1.14 ± 0.16	23.9
PPA-treated (50 h)	1.31 ± 0.25	42.2
PPA-treated (100 h)	1.64 ± 0.13	78.3
Halloysite (10 wt.%)–epoxy		
PA-treated, mixing [9] ^b	1.39	51.1
PA-treated, ball mill [9] ^b	1.39	51.1
Silane-treated, ball mill [9] ^b	1.29	40.2
CTAC-treated, ball mill [9] ^b	1.22	32.6
Clay (10 wt.%)–epoxy [24] ^a	1.13	52.7
Clay (2.5 wt.%)–epoxy [2] ^a	1.26	80.0

^a Measured by SENB.

^b Measured by CT.

values increased to 1.31 MPa m^{1/2} (42.2%) and 1.64 MPa m^{1/2} (78.3%) respectively.

3.3. Toughening mechanisms

The fracture surfaces of the neat epoxy and the halloysite–epoxy composites were comparatively examined using SEM, and some typical micrographs are shown in Figs. 9 and 10. The fracture surface of the neat epoxy was very smooth except for some river-line marks near the crack initiation site, as shown in Fig. 9a. The featureless crack surface indicates the absence of significant plastic shear deformation, highlighting a typical feature of brittle fracture behavior and accounting for the low fracture toughness of the unfilled epoxy.

In contrast to the neat epoxy, the fracture surfaces of the halloysite–epoxy composites show considerably different morphologies, shown in Figs. 9b–e, where much rough surface can be seen. The increased surface roughness implies that the cracking path was deflected because of the presence of the rigid particles, making crack propagation more difficult. With the use of intercalated halloysite particles further increases in surface roughness can be seen, due to the improved dispersion of halloysite particles in the epoxy.

As shown in Figs. 9b–e and Fig. 10, some halloysite agglomerates in the micron scale can be seen on the fracture surfaces of the halloysite–epoxy composites, particularly the fracture surface of the composite with the as-received halloysite. The composites manifest small crack trajectories that are deflected and meander through the matrix, giving rise to the increased resistance to crack propagation. The particle agglomerates may also promote premature tensile failure ahead of crack [8]. In addition to individual particles and particle agglomerates, most of the halloysite particles in the halloysite–epoxy composites with the as-received halloysite are in the form of particle clusters, as shown in Fig. 11a. Halloysite particle clusters can interact with a crack, bridging the crack when

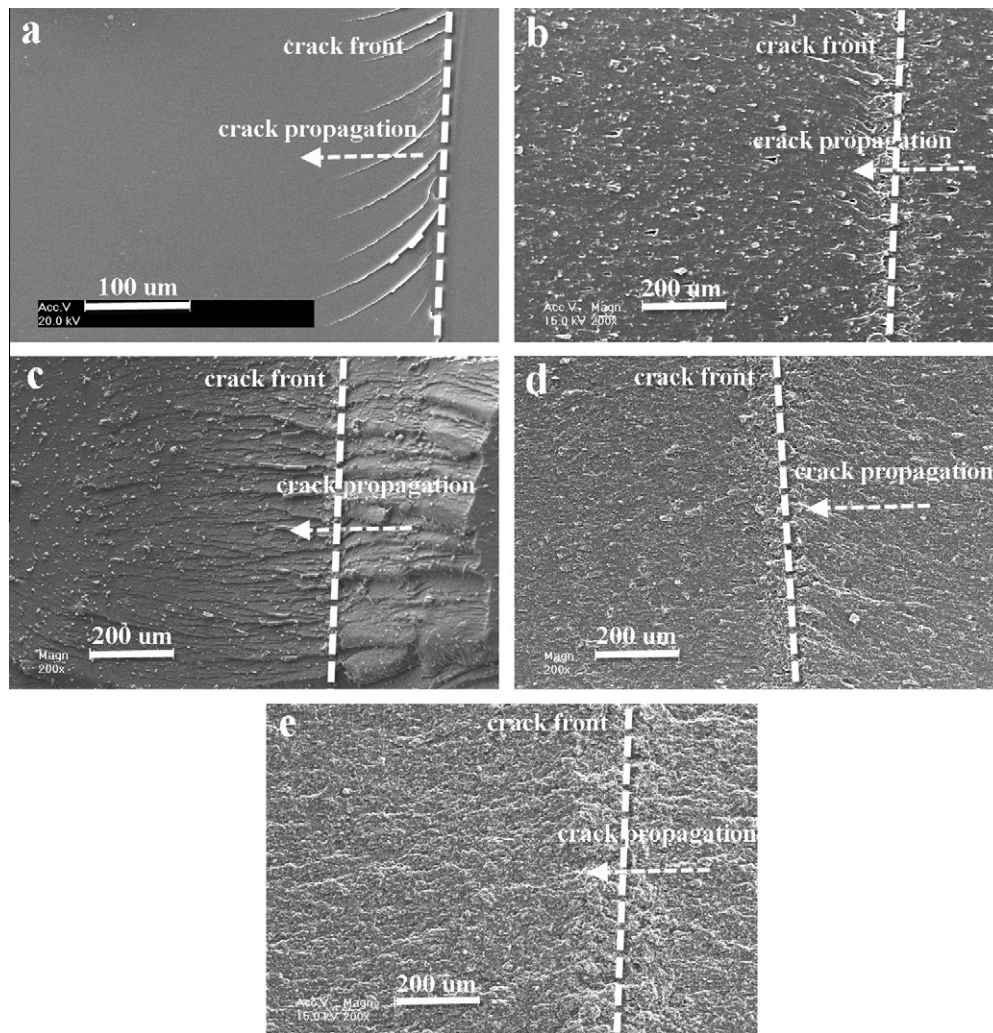


Fig. 9. SEM micrographs of fracture surfaces of CT specimens of neat epoxy and halloysite–epoxy composites. (a) neat epoxy, (b) with as-received halloysite, (c) with 25-h PPA-treated halloysite, (d) with 50-h PPA-treated halloysite, and (e) with 100-h PPA-treated halloysite.

it passes through, resisting the advance of the crack and thus resulting in an increase in fracture toughness [8,9]. Therefore, plastic deformation of the epoxy around particle clusters and crack deflection through the clusters are the dominant toughening mechanisms. Furthermore, the individual halloysite nanotubes, though tiny, have crack front pinning or bridging effects and can also play roles of fiber breakage, fiber debonding and pull-out, which would consume extra energy and increase the resistance to crack initiation and propagation in the halloysite–epoxy composites, as shown in Fig. 11b [9].

For the composites with intercalated halloysite particles, in addition to the abovementioned mechanisms, the increased toughening may be attributed to mechanisms similar to intercalated or exfoliated organoclay in epoxy matrices. Wang et al. [2] showed in exfoliated MMT–epoxy nanocomposites that most micro-cracks are initiated within the intergallery of clay layers rather than at the epoxy–clay interface. Kim and co-workers [22] conducted *in situ* tensile tests of layered silicate/polyamide-12 nanocomposites under an electron microscope and observed that the deformation began inside the stacked silicate layers, and then microvoids formed between the silicate layers. The weakly bonded silicate layers were believed to be sources of the nucleation of micro-cracks. PPA-treated halloysite is also a layered clay mineral, but with each layer bearing no charge due to the absence of isomorphous substitution in either octahedron or tetrahedron sheet. The layers are held

together by hydrogen bonding between hydroxyl groups in the octahedral sheets and oxygen in the tetrahedral sheets of the adjacent layers. Therefore, it is relatively easier for halloysite to be intercalated and dispersed in polymeric matrix than MMT. It has been reported that a number of salts and organic compounds, such as potassium acetate (PA), formamide (FA), hydrazine, etc., were able to intercalate halloysite [16].

Fig. 12 shows TEM micrographs of fracture surfaces of CT specimens of as-received and PPA-treated halloysite–epoxy composites. To show the interactions between crack tip and halloysites, the TEM sections were taken from the vicinity in front of the arrested crack tip in specimens with 90% of individual average peak load for unstable fracture. In the as-received halloysite–epoxy composite the advancing crack was confronting a halloysite cluster, causing multiple cracks at the interfaces between halloysites and the matrix within the cluster, as shown in Fig. 12a. In the intercalated halloysite–epoxy composite the advancing crack was confronting layers of halloysites, causing multiple cracks at the interfaces between halloysite layers and matrix, as shown in Fig. 12c. Microvoids and micro-cracks were found in the treated halloysite–epoxy composites, with micro-cracks forming along the matrix–halloysite interfaces, as shown in Fig. 12c and d, further confirming the observation in SEM (Fig. 11d). In addition, the morphology of the treated halloysite is similar to that of layered silicates. Some intercalated halloysite layers stay together, lying

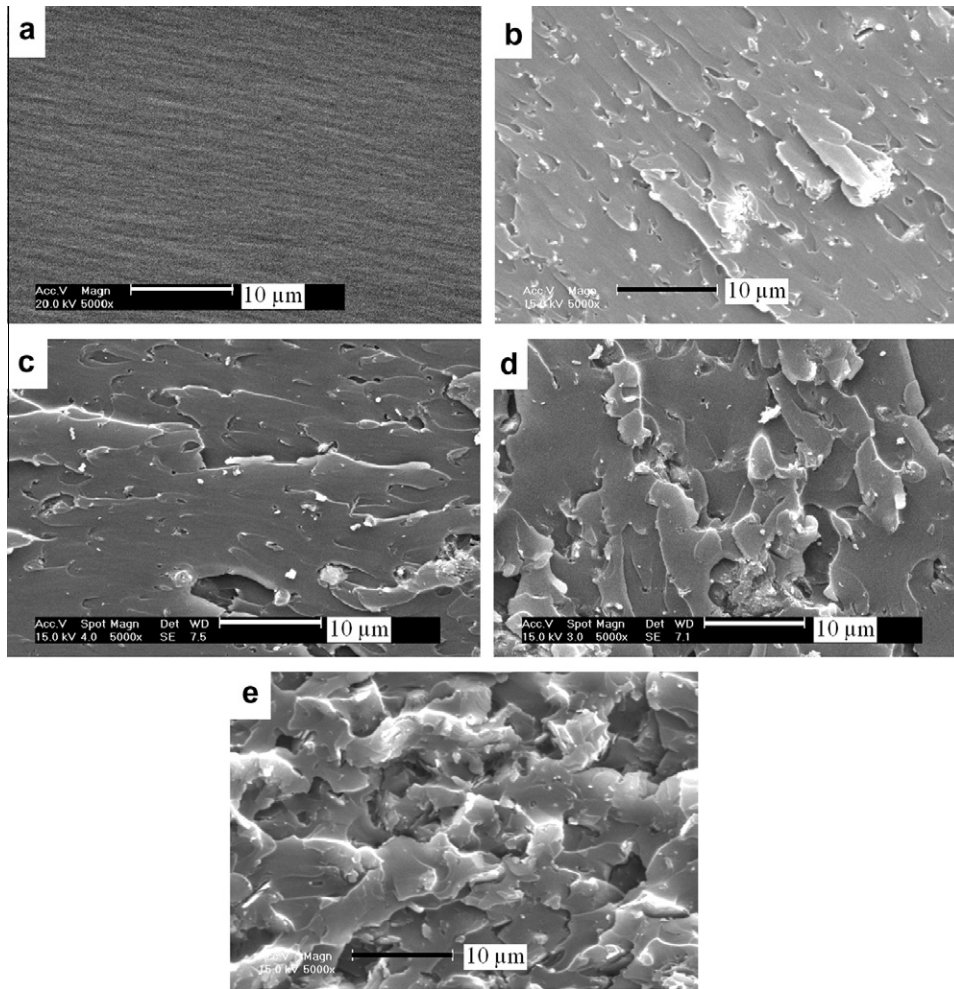


Fig. 10. SEM micrographs of fracture surfaces of CT specimens of neat epoxy and halloysite–epoxy composites near crack tips. (a) neat epoxy, (b) with as-received halloysite, (c) with 25-h PPA-treated halloysite, (d) with 50-h PPA-treated halloysite, and (e) with 100-h PPA-treated halloysite.

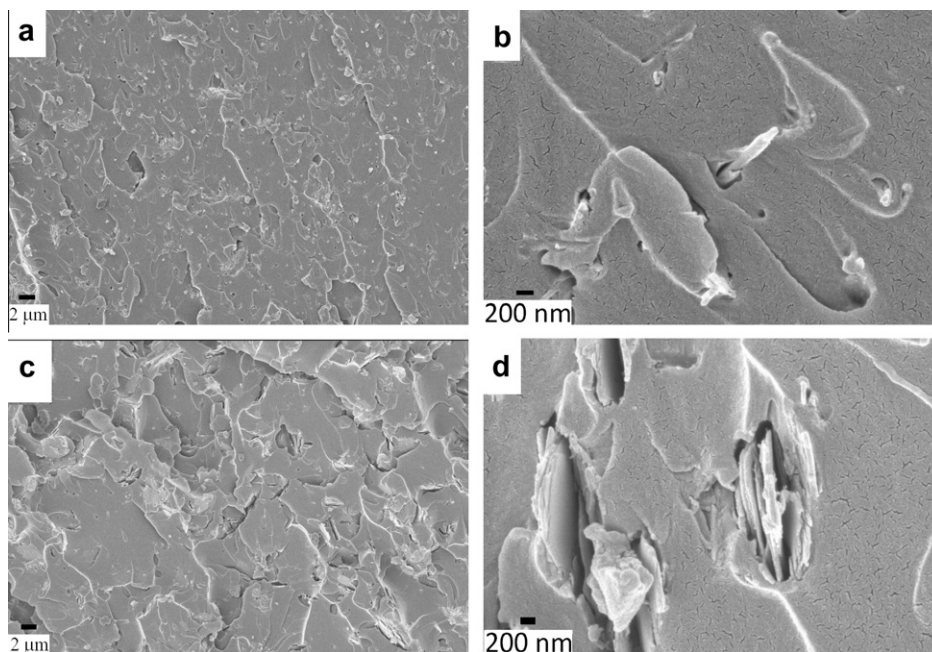


Fig. 11. SEM micrographs with different magnifications of fracture surfaces of CT specimens of (a and b) as-received halloysite–epoxy composite and (c and d) 100-h PPA-treated halloysite–epoxy composite.

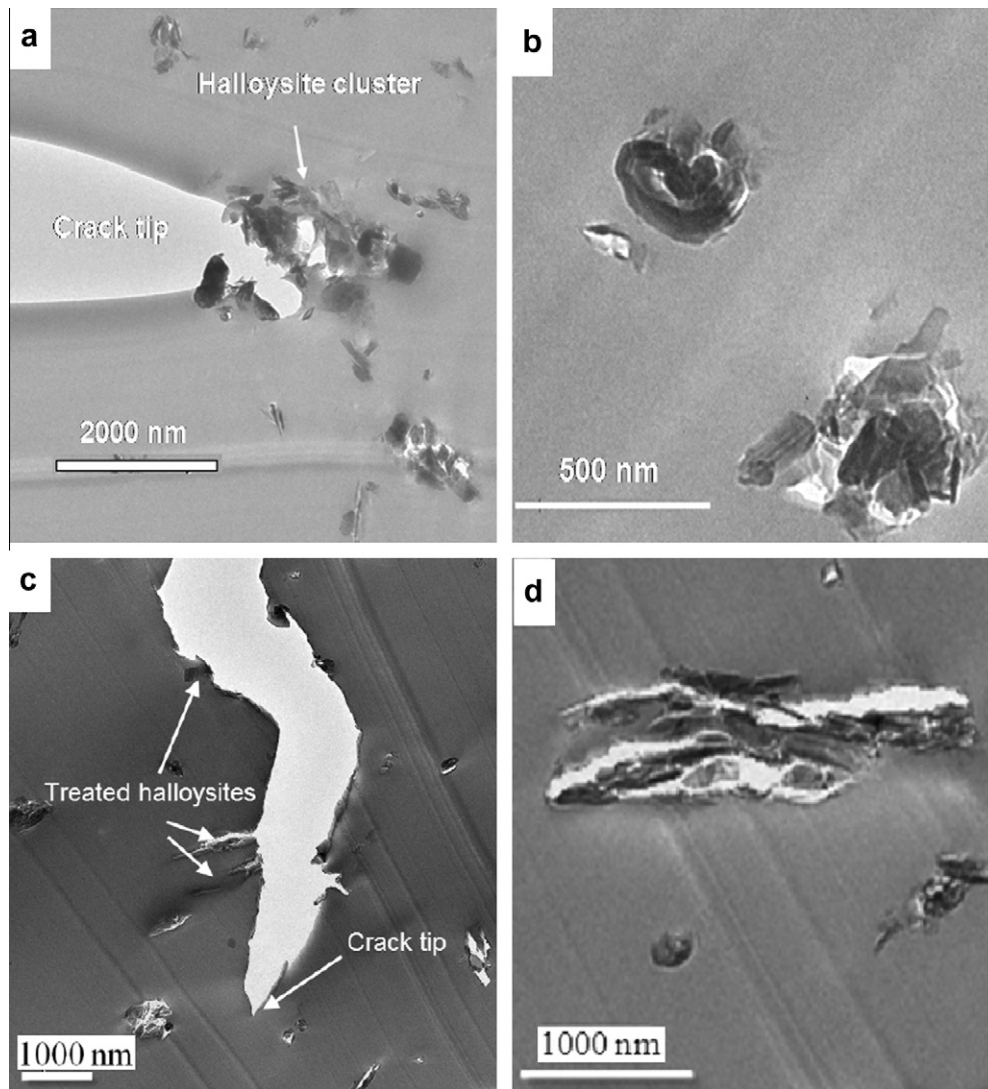


Fig. 12. TEM micrographs of fracture surfaces of CT specimens of (a) and (b) as-received halloysite-epoxy composite; (c) and (d) 100-h PPA-treated halloysite-epoxy composite.

parallel or vertical to the microtomed thin film. Micro- or nano-voids/cracks may promote shear yielding of the epoxy matrix at the crack propagation tips and also throughout the entire volume, absorbing more energy before cracking. The shear yielding of the matrix is associated with several kinds of surface features (such as “lance”, “river” and “hackles”) contributing to an increase in roughness, observed similarly in other epoxy composites [23]. Therefore, both the formation of micro- or nano-voids/cracks and the occurrence of shear yielding contribute to the increase of fracture toughness in the epoxy-halloysite nanocomposites.

Table 3 shows the fracture toughness (K_{IC}) of the neat epoxy and epoxy composites with PPA-treated halloysites as well as other halloysites or organoclays, i.e. potassium acetate (PA) treated or Z6020 silane treated or cetyl trimethyl ammonium chloride (CTAC) treated halloysite (10 wt.)/epoxy composites [9], in which these chemicals improved dispersion but not intercalation, and organoclay (10 wt.)/epoxy composite [24] and s-clay (2.5 wt.)/epoxy composite [2]. Among these, the 100-h PPA-treated halloysite/epoxy composite has the highest K_{IC} value. The unfolded and intercalated halloysite-epoxy composites reported here have a synergistic effect, combining mechanisms exhibited in the tubular-halloysite-epoxy composites and organoclay-epoxy composites. In particular, unfolded platelets exhibit mechanisms similar

to those found in clays, but the absence of charge between layers makes it easy for them to disperse into highly viscous epoxy to form well-dispersed composites. With the use of intercalated halloysite, as a result of the expanded basing space, the rolled halloysite tubes (Fig. 12b) could become flat platelets (Fig. 12d), creating additional particle surfaces due to the release of some internal surface areas concealed by the rolled layers of the nanotubes. The increased halloysite-epoxy contact surfaces could provide extra sites for interactions between halloysite and epoxy matrix under stress. The improved dispersion of halloysite particles in the epoxy due to PPA intercalation contributed to a further increase in the fracture toughness of the halloysite-epoxy composites compared with that of the composite with the non-intercalated halloysite. It can be observed that micro-cracks at the halloysite-epoxy interfaces in the composites were off or even perpendicular to the fracture surface. This implies that the intercalated halloysite particles acted as stress concentrators, promoting a large number of micro-cracks and plastic deformations when the specimen was loaded. The initiation and propagation of micro-cracks occurred at epoxy-halloysite interfaces to form micro- or nano-voids, which would consume more energy than if they emanated only from layer intergallery (hydrogen bonding only) locations, e.g. clays in epoxy [2,24].

4. Conclusion

Phenylphosphonic acid (PPA) was successfully used in this study to unfold and intercalate halloysite, resulting in an increase of basal spacing from 7.2 Å to 15.1 Å, accompanied by the morphology change of most particles from nanotubes to nano-platelets. The halloysite particles were combined with an epoxy to form partially and fully intercalated nanocomposites. It was found that better dispersion in the epoxy was achieved using the unfolded and intercalated halloysite than using the as-received halloysite. There was a significant increase in fracture toughness for the epoxy composites with unfolded and intercalated halloysite particles, without sacrificing other properties such as strength, modulus, glass transition temperature and thermal stability. The fracture toughness of the halloysite–epoxy composites was markedly increased with an increase in the intercalation levels. The improvement in K_{1C} for the composite containing 100-h PPA-treated halloysite particles was 78.3%.

In the halloysite–epoxy composite with the as-received halloysite particles, in which the predominant particle shape was tubular, the increase in fracture toughness was due mainly to mechanisms such as crack bridging, crack deflection and plastic deformation of the matrix around the halloysite particle clusters, fiber breakage, fiber debonding and pull-out of individual halloysite nanotubes in the composite. In the composites with the unfolded and intercalated halloysite there was a substantial increase in the total contact area between halloysite and epoxy, as a result of the morphology change from nanotubes to nano-platelets. This feature, together with the improved dispersion of the halloysite particles in the epoxy due to PPA intercalation, increased the fracture toughness of the composite beyond that of the as-received halloysite–epoxy composite. Meanwhile, micro-cracks initiated at the halloysite–epoxy interfaces in the composites with the intercalated halloysite, resulting in higher fracture toughness of the intercalated halloysite–epoxy nanocomposites than that of organoclay–epoxy nanocomposite.

Acknowledgements

L. Ye and Y.H. Tang are grateful for the support of the Australian Research Council (ARC) with a Discovery Project (DP) Grant (No.: DP0880433) for the research work.

References

- [1] Basara G, Yilmazer U, Bayram G. Synthesis and characterization of epoxy based nanocomposites. *J Appl Polym Sci* 2005;98:1081–6.

- [2] Wang K, Chen L, Wu JS, Toh ML, He CB, Yee AF. Epoxy nanocomposites with highly exfoliated clay: mechanical properties and fracture mechanisms. *Macromolecules* 2005;38:788–800.
- [3] Wang JG, Fang ZP, Gu AJ, Xu LH, Liu F. Effect of amino-functionalization of multi-walled nanotubes on the dispersion with epoxy resin matrix. *J Appl Polym Sci* 2006;100:97–104.
- [4] Fidelus JD, Wiesel E, Gojny FH, Schulte K, Wagner HD. Thermo-mechanical properties of randomly oriented carbon/epoxy nanocomposites. *Composites Part A – Appl Sci* 2005;36:1555–61.
- [5] Deng SQ, Ye L, Friedrich K. Fracture behaviors of epoxy nanocomposites with nano-silica at low and elevated temperatures. *J Mater Sci* 2007;42:2766–74.
- [6] Horvath E, Kristof J, Frost RL, Redey A, Vagvolgvi V, Cseh T. Hydrazine-hydrate intercalated halloysite under controlled-rate thermal analysis conditions. *J Therm Anal Calorim* 2003;71:707–14.
- [7] Ye YP, Chen HB, Wu JS, Ye L. High impact strength epoxy nanocomposites with natural nanotubes. *Polymer* 2007;48:6426–33.
- [8] Deng SQ, Zhang JN, Ye L, Wu JS. Toughening epoxies with halloysite nanotubes. *Polymer* 2008;49:5119–27.
- [9] Deng SQ, Zhang JN, Ye L. Halloysite–epoxy nanocomposites with improved particle dispersion through ball mill homogenisation and chemical treatments. *Compos Sci Technol* 2009;69:2497–505.
- [10] Shi XM, Nguyen TA, Suo ZY, Liu YJ, Avci R. Effect of nanoparticles on the anticorrosion and mechanical properties of epoxy coating. *Surf Coat Technol* 2009;204:237–45.
- [11] Liu MX, Guo BC, Du ML, Lei YD, Jia DM. Natural inorganic nanotubes reinforced epoxy nanocomposites. *J Polym Res* 2008;15:205–12.
- [12] Li CP, Liu JG, Qu XZ, Guo BC, Yang ZZ. Polymer-modified halloysite composite nanotubes. *J Appl Polym Sci* 2008;110:3638–46.
- [13] Liu MX, Guo BC, Du ML, Cai XJ, Jia DM. Properties of halloysite nanotube–epoxy resin hybrids and the interfacial reactions in the systems. *Nanotechnology* 2007;18:455703.
- [14] Jia ZX, Luo YF, Guo BC, Yang BT, Du ML, Jia DM. Reinforcing and flame-retardant effects of halloysite nanotubes on LLDPE. *Polym-Plast Technol* 2009;48:607–13.
- [15] Du ML, Guo BC, Jia DM. Thermal stability and flame retardant effects of halloysite nanotubes on poly(propylene). *Eur Polym J* 2006;42:1362–9.
- [16] Joussein E, Petit S, Churchman J, Theng B, Righi D, Delvaux B. Halloysite clay minerals – a review. *Clay Miner* 2005;40:383–426.
- [17] Frost RL, Kristof J. Intercalation of halloysite: a Raman spectroscopic study. *Clay Clay Miner* 1997;45:551–63.
- [18] Joussein E, Petit S, Delvaux B. Behavior of halloysite clay under formamide treatment. *Appl Clay Sci* 2007;35:17–24.
- [19] Xiao KQ, Ye L, Kwok YS. Effects of pre-cracking methods on fracture behavior of an Araldite-F epoxy and its rubber-modified systems. *J Mater Sci* 1998;33:2831–6.
- [20] Yuan P, Southon PD, Liu ZW, Green MER, Hook JM, Antill SJ, et al. Functionalization of halloysite clay nanotubes by grafting with gamma-aminopropyltriethoxysilane. *J Phys Chem C* 2008;112:15742–51.
- [21] Brunauer S, Emmert PH, Teller E. Adsorption of gases in multimolecular layers. *J Am Chem Soc* 1938;60:309–19.
- [22] Kim GM, Lee DH, Hoffmann B, Kressler J, Stoppelman G. Influence of nanofillers on the deformation process in layered silicate/polyamide-12 nanocomposites. *Polymer* 2001;42:1095–100.
- [23] Liu TX, Tjiu WC, Tong YJ, He CB, Goh SS, Chung TS. Morphology and fracture behavior of intercalated epoxy/clay nanocomposites. *J Appl Polym Sci* 2004;94:1236–44.
- [24] Brunner AJ, Nicola A, Rees M, Gasser P, Kornmann X, Thomann R, et al. The influence of silicate-based nano-filler on the fracture toughness of epoxy resin. *Eng Fract Mech* 2006;73:2336–45.